*Particle Accelerators*, Vol. 59, pp. 75–92
Reprints available directly from the publisher
Photocopying permitted by license only



# THE END MAGNETS OF THE IFUSP RACE-TRACK MICROTRON BOOSTER

L.R.P. KASSAB[a,*], P. GOUFFON[b], M.N. MARTINS[b] and J. TAKAHASHI[b]

[a]*Faculty of Technology, CEETPS-UNESP, SP, Brazil;* [b]*Linear Accelerator Laboratory, Institute of Physics, University of São Paulo, C.P. 66318, 05315-970, São Paulo, SP, Brazil*

*(Received 7 April 1997; In final form 8 October 1997)*

The end magnets of the IFUSP race-track microtron booster, second stage of the electron accelerator under construction at the Linear Accelerator Laboratory, are presented. They deflect, focus and return the beam to the accelerating section. Details about the project are discussed. Poisson code was used to give the final geometry of the end magnets. The end magnets incorporate auxiliary pole pieces (clamps) which create a reverse fringe field region that avoids the beam vertical defocusing and reduces the horizontal displacement produced by extended fringe fields (EFF). The small gap height used for the clamps provided reverse field distributions with fringe fields of short extensions, avoiding the traditional use of inactive clamps. Measurements and calculations concerning particle trajectories and reverse field distribution are presented. The floating wire technique, employing an original procedure to register orbits, was used to corroborate the calculated beam trajectories and represents a good experimental option in the lack of the accelerator beam. The experimental results showed agreement of about 0.1% with the calculations.

*Keywords:* IFUSP race-track; Magnets; Microtrons; Floating wire; Reverse fringe field

## 1 INTRODUCTION

The cw race-track microtron[1] electron accelerator under construction at IFUSP will have three stages (Figure 1). The first one, with input energy of 100 keV and output energy of 1.97 MeV, is composed of two accelerating sections with lengths of 1.00 and 1.47 m. The second stage, where the energy will be raised from 1.97 to 5.1 MeV, called microtron

* Corresponding author. Fax: (55) (011) 2108668. E-mail: lpires@if.usp.br.

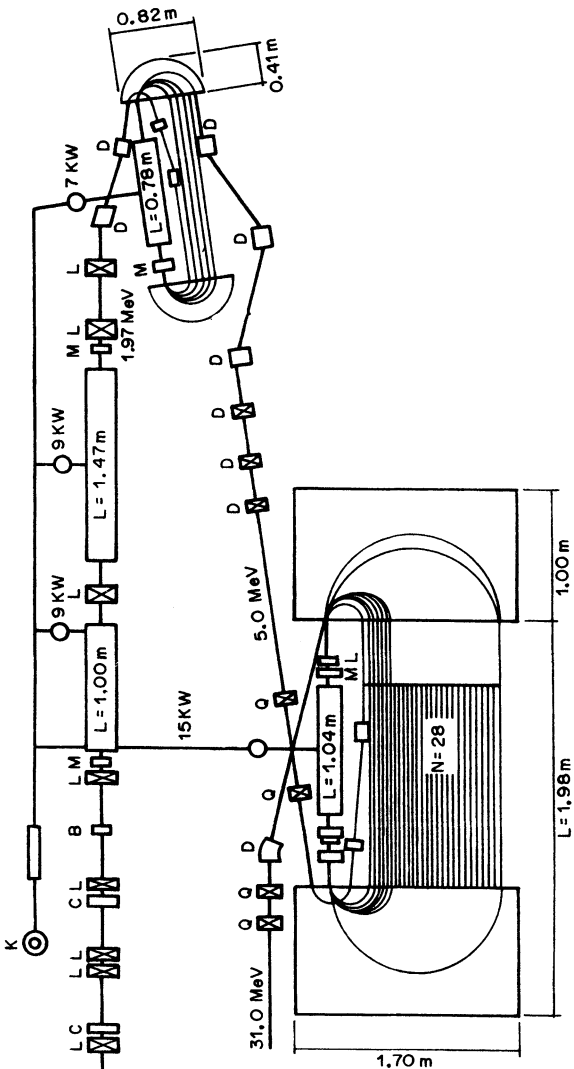


FIGURE 1 Schematic view of the IFUSP RTM. K: klystron valve; G: electron gun; B: buncher; C: chopper cavities; L: solenoid lenses; Q: quadrupole lenses; D: deflecting dipoles; and M: beam monitors.

TABLE I IFUSP race-track microtron booster parameters

| | |
|---|---|
| Injection energy | 1.97 MeV |
| Output energy | 5.10 MeV |
| Accelerating microwave | 12.1 cm |
| Energy gain per turn | 0.63 MeV |
| Total number of orbits | 5 |
| Radius of the injection orbit | 7.77 cm |
| Radius of the first orbit | 9.82 cm |
| Radius of the last orbit | 18.20 cm |
| Magnetic field | 0.1020 T |
| Average beam current | 50 μA |
| Distance between the magnets | 138 cm |

booster, consists of an accelerating section (0.78 m) and two end magnets ($B = 0.1020$ T), in which the beam will circulate five times. In the third stage, after 28 turns, a beam of 31 MeV will be delivered. Table I presents the main parameters of the microtron booster.

This work deals with solutions concerning the design of the second stage end magnets, the reverse field distribution, orbit calculations and measurements employing the floating wire technique.[2]

## 2 THE END MAGNETS

The end magnets play a fundamental role in terms of the beam quality. Their efficiency depends on the behavior of the magnetic fields that deflect, focus and return the beam to the accelerating section. The absence of a required uniformity in the magnetic field or the presence of inadequate fringe fields destroys the synchronism between the returning beam bunch and the accelerating microwave.

### 2.1 Field Requirements

The resonance condition, $2\pi \Delta E/qBc^2 = \nu T_{RF}$, determines in first order the magnetic field. The energy gain in the accelerating structure is $\Delta E$, $q$ is the charge of the particle being accelerated, $B$ is the magnetic field in the bending magnets, $c$ is the velocity of the light in vacuum and $\nu$ is a multiple integer of the radiofrequency period $T_{RF}$. Setting $\nu = 1$ allows the least stringent tolerances in terms of the synchronous phase $\phi_s$ and optimizes the number of captured particles, as $0 < \tan\phi_s < 2/\pi\nu$. The

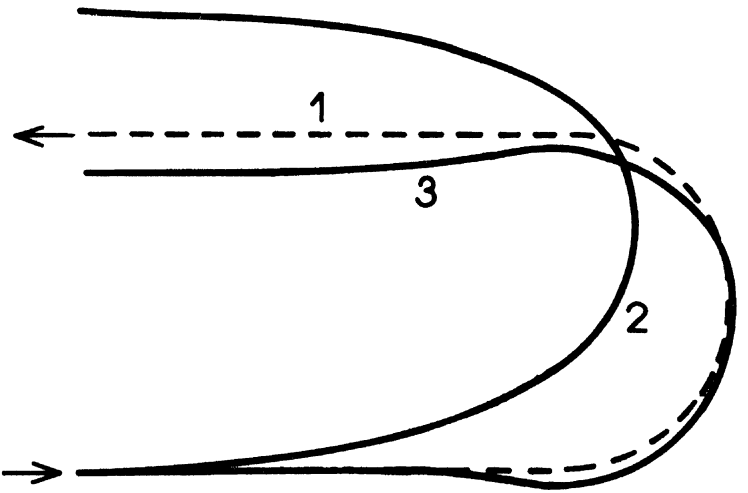


FIGURE 2 Beam trajectories for different magnetic field distributions: (1) hard edge field; (2) EFF – extended fringe field; (3) reverse fringe field.

resonance condition is obtained under the assumption that the magnetic field is uniform and, at the magnet edge, falls to zero abruptly (hard edge field). In this case, the ideal trajectory would be composed of two straight line segments and a semi-circle in the region of the uniform field (Figure 2, curve 1). However, the magnet sectors have extended fringe fields (EFF) that distort the orbits, causing vertical defocusing and horizontal displacement (Figure 2, curve 2) that compromise the synchronism. As the trajectory is altered, the orbit period changes, the beam does not meet the accelerating microwave in the correct phase and the energy is changed. So the resonance condition is hardly fulfilled in these conditions. Through the use of active clamps[3] (auxiliary pole pieces shown in Figure 3(b) with opposite excitation to that of the main poles), that provides a reverse fringe field region (Figure 3(a)), the effects associated with EFF[4,5] are eliminated and the orbits (Figure 2, curve 3) get close to the ideal ones. The field distributions shown in Figure 3(a) were simulated using Poisson[6] code for the cross-section, exhibited in Figure 3b, with and without the clamps. These field distributions were used for the trajectory calculations with the Ptrace[7] code that performs numerical integration in the fringe field region.

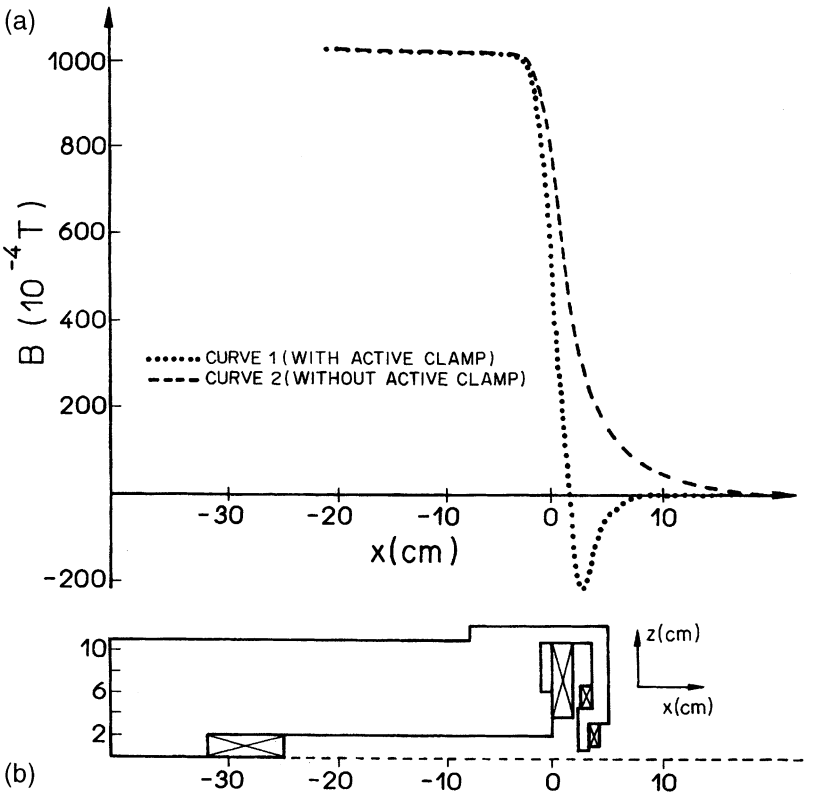


FIGURE 3 (a) Magnetic field distributions, calculated with Poisson code, as a function of the distance to the pole edge (curve 1 – reverse fringe field; curve 2 – extended fringe field). (b) Half vertical cross-section of the microtron booster accelerator end magnet with the active clamp.

Calculations with the Poisson and Ptrace codes were necessary to adjust the profile of the clamps to a feasible geometry whose field distribution enables the particle acceleration.

H.A. Enge[4,5] presents in his paper the effect of the EFF to the trajectory of a particle. As the intensity of the magnetic field normal component gradually increases in a EFF (the tangential component is null for symmetry), when the particle, situated at the middle plane, comes into the field region, its trajectory radius gradually decreases. On the other hand, when it leaves the field, the radius increases. In our

case, from the ideal trajectory ($y = 0$), we observe beam displacements of 1.62 cm for the injection orbit (Figure 4(a)) and of 0.69 cm for the fifth one (Figure 4(b)). These results can be compared to those, significantly smaller, that occur in the reverse fringe field region of the end magnets (0.33 cm for the injection orbit and 0.14 cm for the fifth one), also shown in Figures 4(a) and 4(b). Details of the particle trajectories, without the injection orbit, are shown in Figure 4(c).

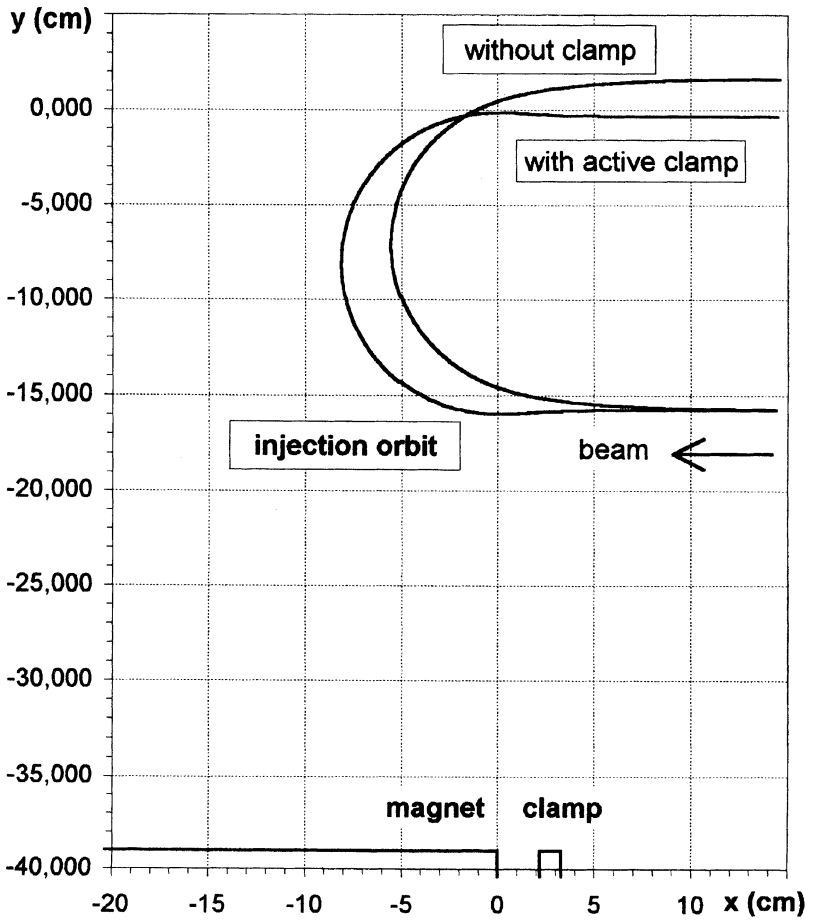


FIGURE 4(a) Trajectories of the injection orbit, in the middle plane, in the presence of the extended fringe field (without clamp) and of the reverse fringe field (with active clamp).

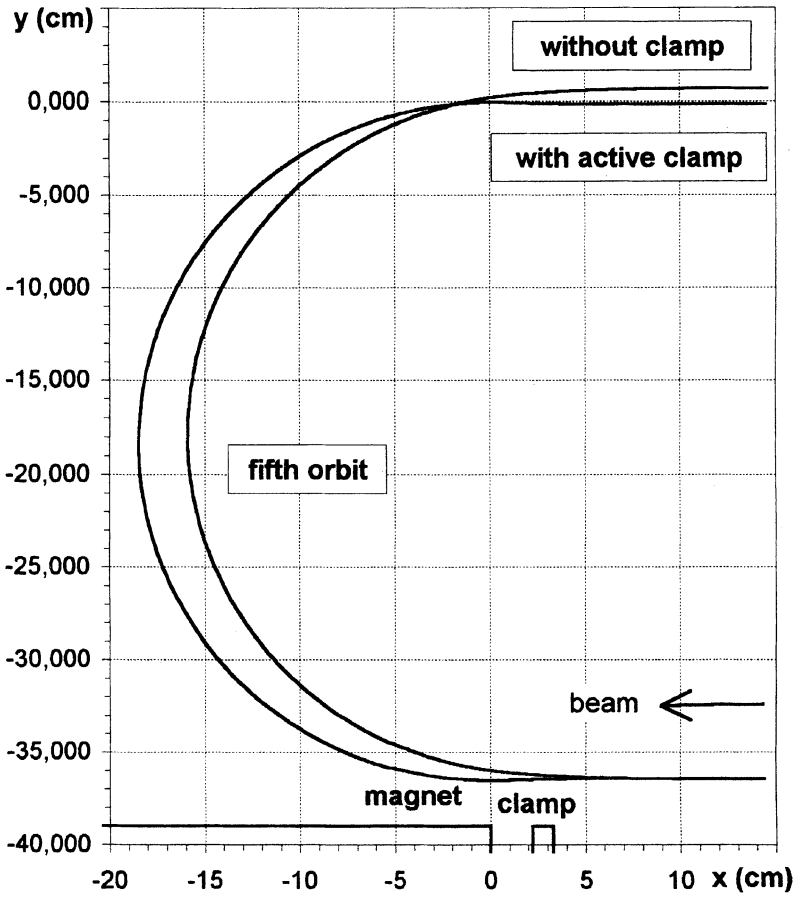


FIGURE 4(b) Trajectories of the fifth orbit, in the middle plane, in the presence of the extended fringe field and of the reverse fringe field.

For the charged particle situated out of the middle plane, in the EFF, there also are vertical defocusing forces due to the interaction with the tangential component of the magnetic field. So the particle comes into the uniform region with a vertical velocity component. These effects also alter the period orbit and compromise the resonance condition. On the other hand, in the reverse fringe field region, the particle is submitted to weak vertical focusing forces and maintain an almost

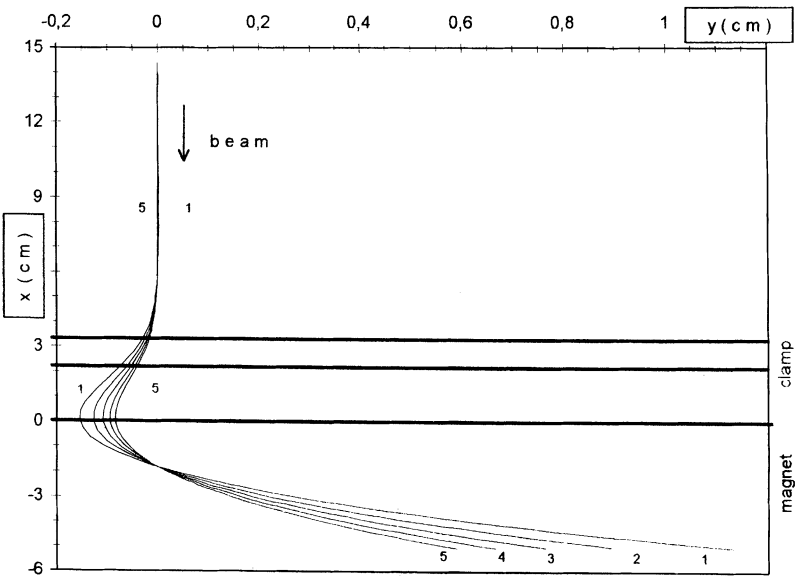


FIGURE 4(c) Trajectories at the entrance of the magnet, in the middle plane, in the presence of the reverse fringe field.

constant distance from the middle plane, during the passage through the fringe field region, instead of moving away from it, as it occurs in the EFF. This is shown in Figures 5(a) and 5(b) that exhibit calculations with Ptrace code for a particle situated 0.1 cm above the middle plane. In the EFF case, as presented in Figure 5(a), vertical displacements of $1870.6 \times 10^{-3}$ mm for the injection orbit and of $470.5 \times 10^{-3}$ mm for the fifth one are observed. For the reverse fringe field, these vertical displacements are of $5.3 \times 10^{-3}$ mm for the injection orbit and of $2.6 \times 10^{-3}$ mm for the fifth one (Figure 5(b)).

Assuming that the reverse fringe field region is symmetric about the middle plane of the magnet ($z = 0$), the vertical focal length $f_z$, for electrons that enter the field at a distance $z$ from the middle plane, is given by:[8]

$$\frac{1}{f_0} + \frac{1}{f_1} = \frac{\int_0^1 (B/B_0)^2 \mathrm{d}x - \int_0^1 (B/B_0)\mathrm{d}x}{r^2} + \frac{2z^2}{3r^2} \int_0^1 \left( \frac{1}{B_0} \frac{\mathrm{d}B}{\mathrm{d}x} \right)^2 \mathrm{d}x,$$

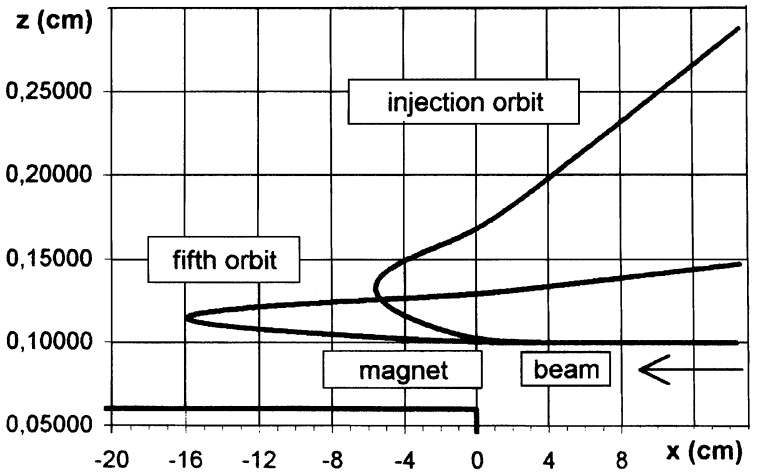


FIGURE 5(a) Injection and fifth orbit's trajectories, at $z = 0.1$ cm, in the presence of the extended fringe field.

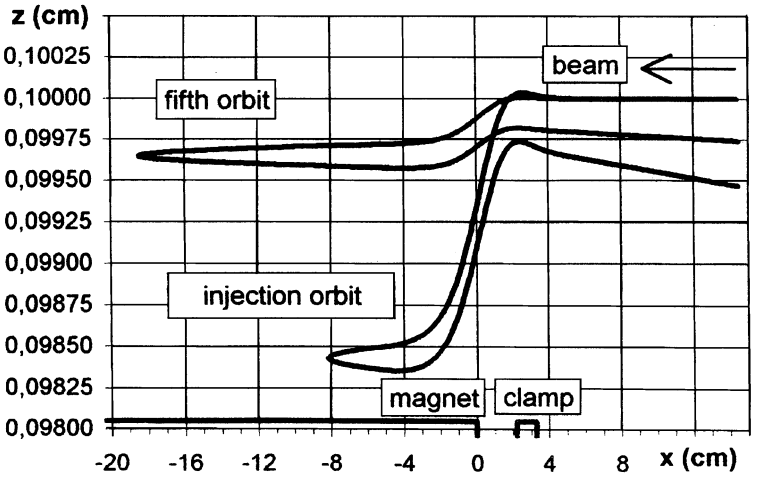


FIGURE 5(b) Injection and fifth orbit's trajectories, at $z = 0.1$ cm, in the presence of the reverse fringe field.

where $x = 0, \ldots, l$ is the fringe field length, $r$ is the curvature radius and $B_0$ is the uniform field.

The focal distance of a particle that is very close to the middle plane is given by $f_0$ and, in this case, the contribution of the second term $1/f_1$ is negligible. The field distribution has to be adequately chosen in order to make $1/f_0 \to 0$. This assures that the trajectory remains parallel to the middle plane. For a particle that is out of the middle plane, the focal distance also depends on the second term $1/f_1$. This term, of second order, is associated with the spherical aberration because of its dependence on $z$ and has to be small. The end magnets reverse fringe field distribution satisfies these requirements, as $1/f_0 = 9.9 \times 10^{-4}\,\mathrm{cm}^{-1}$ and $1/f_1 = 4.7 \times 10^{-5}\,\mathrm{cm}^{-1}$ for a particle of the injection orbit ($r = 7.77$ cm) with $z = 0.1$ cm.

It can be shown[8] that, for a particle that is out of the middle plane, the horizontal displacement also depends on a second order term, given by $z^2/2r$, that is related to the vertical position. For the injection orbit of a particle with $z = 0.1$ cm, this term would provide a contribution of $6.5 \times 10^{-4}$ cm to the horizontal displacement. So, this second order term gives the difference between the horizontal displacement of a middle plane trajectory ($z = 0$) and the one in another plane ($z \neq 0$).

There is another field configuration proposed by Froelich and Manca[1] (University of Western Ontario) that also satisfies the conditions above. However, in this case, the magnets exhibit a "ridge" field at the edge and achieves radial and vertical focusing by means of different gap heights. The practical realization of specific field profiles is difficult and, consequently, most RTM designers have preferred to separate the functions of bending and focusing. The use of active clamps, first suggested by Babic and Sedlacek (1967), is now incorporated into almost all race-track microtron designs.

The magnets must provide uniform field distribution of about $\Delta B/B = 10^{-3}$ over the area occupied by the trajectories. Changes of the magnetic field produce variations of the path length, given by $\Delta B/B = \Delta L/L$, and of the microwave phase angle where the electron is accelerated:

$\Delta\phi_{\mathrm{RF}}/360^\circ = \Delta L/\lambda_{\mathrm{RF}}$ ($\Delta L$ = orbit length change, $\lambda_{\mathrm{RF}}$ = accelerating microwave = 12.1 cm).

Using both equations we obtain: $\Delta B/B = \lambda_{\mathrm{RF}}\Delta\phi_{\mathrm{RF}}/360^\circ \pi r$. Considering the fifth orbit radius, $r = 18.202$ cm and $\Delta\phi_{\mathrm{RF}} = 1^\circ$, the

TABLE II Characteristics of the orbits in the booster as calculated by Ptrace

| *Orbit* | *Radius* (cm) | *Energy* (MeV) | *Orbit separation in the uniform field region* (cm) |
|---|---|---|---|
| 1 | 9.822 | 2.575 | $d_{12}=4.224$ |
| 2 | 11.934 | 3.207 | $d_{23}=4.196$ |
| 3 | 14.032 | 3.838 | $d_{34}=4.172$ |
| 4 | 16.118 | 4.469 | $d_{45}=4.168$ |
| 5 | 18.202 | 5.100 | |

required uniformity is given by $\Delta B/B=0.06\%$. For the first orbit, $r=9.822$ cm and $\Delta B/B=0.11\%$.

The correction of the magnetic field was done attaching to the pole faces coils made of etched printed circuit boards[9,10] that provides uniformity of $\Delta B/B=10^{-5}$, much better than the one required for the machine operation.

The separation between the return paths of consecutive orbits is large enough to enable the installation of correcting lenses. Assuming $\beta=1$ ($\beta=v/c$) and considering the width of the fringe field negligible (hard edge field), we obtain for the distance between the orbits an approximate constant value given by $d=v\lambda_{RF}/\pi\approx 3.9$ cm. More realistic orbit calculations are done by the Ptrace code, that considers the effects of the reverse fringe fields and the velocity of the electron in each turn. The results presented in Table II show that the distances between consecutive orbits are not constant and tend to the theoretical value as the beam energy increases.

## 2.2 The Design of the End Magnets

The size of the magnets depends on the radius of the last orbit because they have to deflect an electron beam of 5.1 MeV in a semi-circular trajectory of about 36 cm diameter, taking also into account the space needed for the coils. The design of the end magnets, without the clamps, is shown in Figure 6. The magnet is mounted from pieces of laminated iron in order to avoid Foucault currents. The two semi-circular pole pieces are identical and separated by a central semi-circular ring; they were precision machined to within 0.01 mm. This care is not enough to avoid the presence of magnetic field tangential components in the pole-gap interfaces. Running Poisson code, considering parallelism for the two smooth pole faces, for the geometry shown in Figure 3(b),

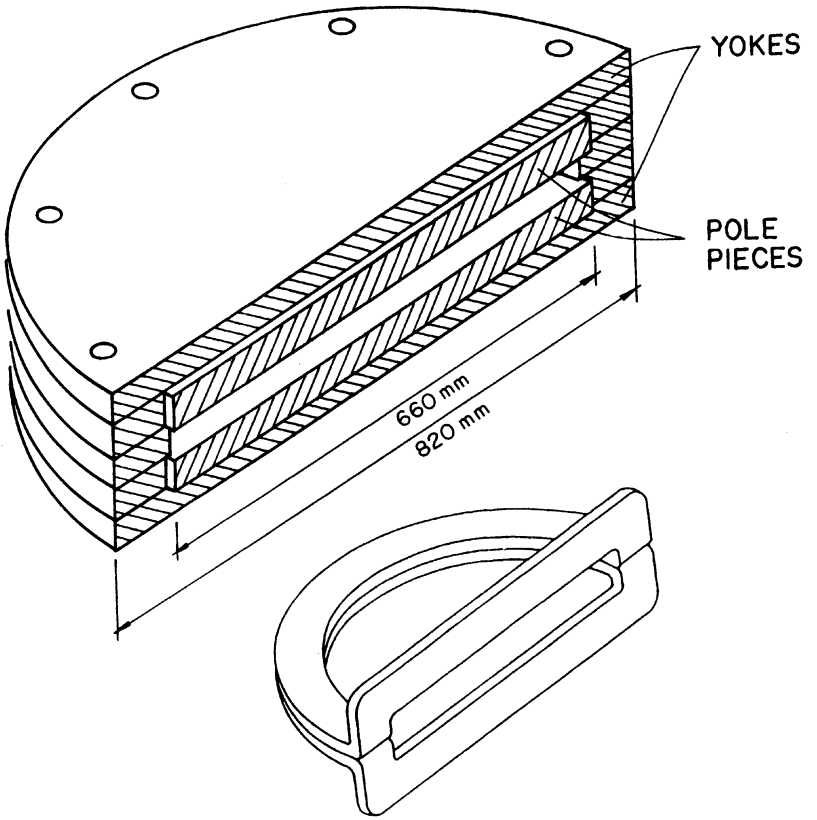


FIGURE 6 The microtron booster end magnets, without the clamps, and the shape of the coils.

variations of 0.13%, in a field of 0.102 T, were observed in the middle plane of the magnet gap. The real inhomogeneities measured[9,10] before the correction of the magnetic field were of $\Delta B/B = 0.15\%$. The gap formed by the semi-circular ring and the pole pieces is a semi-cylindrical volume with 4.0 cm height and 64.0 cm diameter. The small gap height chosen provides advantages as less extensive fringe fields, higher magnetic fields for the same dissipated power and more uniform field distribution. The coils (Figure 6), constructed with copper wire of 4.6 mm diameter arranged in 4 layers of 15 turns each, present an electrical resistance of 0.127 Ω, have an original geometry and involve the pole pieces in an unusual way. The power dissipated in each coil is

TABLE III Coil parameters of the end magnets

| | *Main coil* | *Reversing coil (clamp)* |
|---|---|---|
| Wire diameter | 4.6 mm | 1.08 mm |
| Number of turns (N) | 60 | 120 |
| Total current (NI) | 1638 A · turns | 250 A · turns |
| Current | 27.3 A | 2.1 A |
| Power | 95 W | 22 W |
| Resistance | 0.127 Ω | 5.0 Ω |

about 95 W, when submitted to a 27.3 A current, necessary to generate a magnetic field of 0.1020 T. Then, an external simple system of forced ventilation succeeds in refrigerating the coils. The clamps produce, as discussed before, reverse fringe field distributions with fringe fields of short extensions. Then inactive clamps, usually employed to reduce the fringe field extension, are not necessary. We should remark that this is related to the atypical solution of leaving the gap with a small height (2.2 cm) that differs from the gap of the magnets (4.0 cm). The nearness between the clamps and the magnets pole pieces (Figure 3(b)) assures, in the region of non uniform magnetic field, a field distribution with short extension that decays to negative values abruptly. Each clamp coil, made with 1.08 mm diameter copper wire disposed in 20 layers of 6 turns, has electrical resistance of 5.0 Ω and dissipates 22 W with the 2.1 A current determined in the calculations. As the clamps are in the neighborhood of the magnet pole pieces, there was no available space to mount the coils around the clamps pole pieces, and this led us to find a different way to arrange them, that is to say, diagonally (Figure 3(b)).

We should say that, in spite of its compact geometry, the end magnets assured the required parameters for the race-track microtron booster operation.

The coil parameters of the end magnets are presented in Table III.

## 2.3 Field Measurements

The fringe fields of the end magnets were measured with a Hall probe[11] that consists of a thin rectangular ($2 \times 5\,mm^2$ area and 1 mm thick) semiconductor wafer. The gaussmeter[12] accuracy is $5 \times 10^{-4}$ of the full range and the measurements were done using five different ranges, from $3 \times 10^{-3}$ to $3 \times 10^{-1}$ T. The measurements were performed in the middle plane, along three lines perpendicular to the pole edges, one of

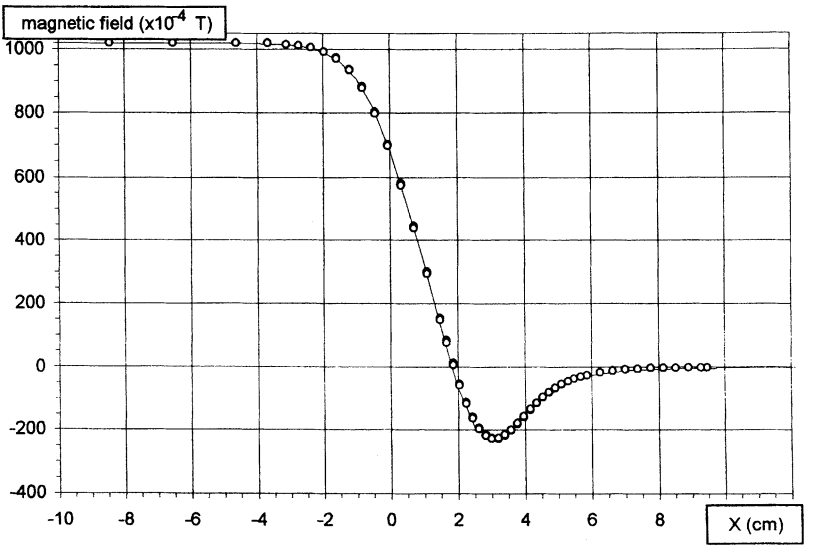


FIGURE 7 Calculated (continuous line) and measured (experimental points) magnetic field distributions for one of the end magnets, as a function of the distance to the pole edge.

them in the middle of the magnet and the other two at 15 cm on each side. Along each line, were measured 50 points, separated by 1.91 mm. The results for one of the magnets are presented in Figure 7. The uncertainties are smaller than the symbols, and the three measurements are plotted together. The curve in Figure 7 shows the field distribution calculated by the Poisson code. There is excellent agreement between the calculated and measured fields.

## 3 DETERMINATION OF THE ORBITS

The calculated orbits were checked employing the floating wire technique. The trajectory of a charged particle $q$ with momentum $p$ in a magnetic field $B$ is equivalent to the shape assumed by a flexible wire carrying a current $i$, submitted to a tension $T$. The current should be high enough to make the wire become incandescent, to increase its flexibility and visibility. The tension is applied by running the wire over a pulley and attaching it to a weight to compensate the magnetic force,

that is: $T/i = Br = p/q$. Friction in the pulley is minimized by the use of compressed air, in its bearings, whose flux must be properly controlled. Cheaper than platinum and gold and with high melting point, it was used a 50 μm diameter nickel wire, very flexible and with small mass in order to reduce the gravitational force. The radii of the first, third and fifth orbits were measured using, respectively, masses of 613.3, 876.3 and 1136.7 mg and a current of 600 mA. These masses were determined, using the equation given above, for the radii obtained by the Ptrace code for a uniform magnetic field of 0.1020 T. Making use of an original experimental procedure, the orbits established by the incandescent wire were registered in paper sheets with the aid of a nonmagnetic mechanical device (Figure 8), with a movable support, specially designed to be inserted in the gap of the end magnets. Figure 9 shows the incandescent wire in one of the end magnets.

Table IV presents a comparison between the radii measured using the floating wire technique (average of five measurements) and those calculated by the Ptrace code. The results show a good agreement (within 0.5%) between measured and calculated values. However, this difference can be explained by the mass of the wire hanging between the pulley and the weight, which was neglected in the calculations.

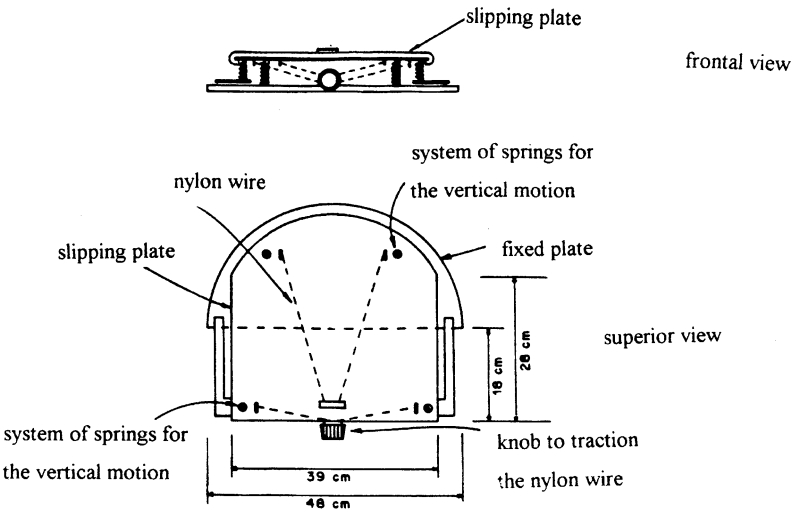


FIGURE 8 Mechanical device to register the floating wire trajectories.

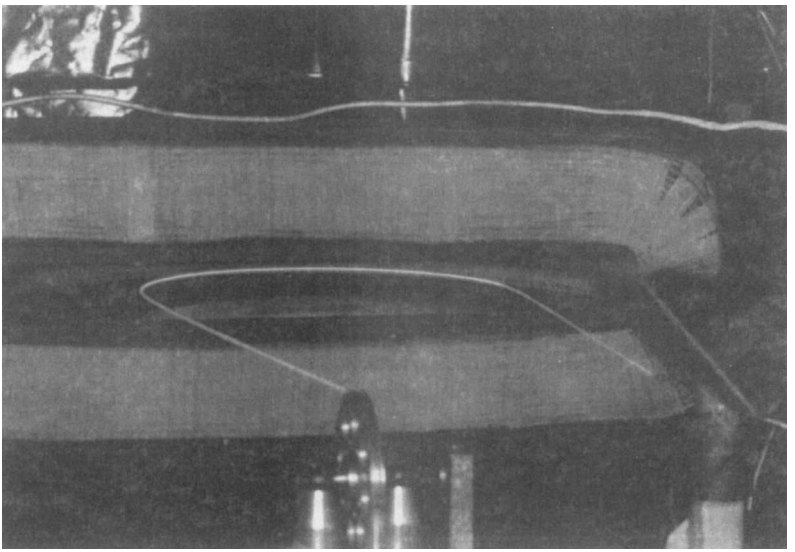

FIGURE 9 The floating nickel wire in equilibrium inside the end magnet gap. (See color plate I).

TABLE IV Measured and calculated radii

| *Orbit number* | *Radius* (cm) | |
|---|---|---|
| | *Calculated by Ptrace* | *Measured by the floating wire (average of 5)* |
| 1 | 9.82 | $9.87 \pm 0.05$ |
| 3 | 14.03 | $14.10 \pm 0.09$ |
| 5 | 18.20 | $18.29 \pm 0.05$ |

Considering this extra mass (of approximately 3.5 mg) the calculated radii agree with the measurements within 0.1%. This result is an assessment of the floating wire technique and assures that the expression above is a good model for the actual physical situation.

It is important to add that the floating wire technique is not conventionally used to measure orbits, due to difficulties of its achievement. However, it represents a good alternative to check the orbits in advance, in the lack of the accelerator beam.

## 4 CONCLUSIONS

The end magnets of the IFUSP race-track microtron booster were designed with the aid of numerical field computations (Poisson code) and of ray-tracing calculations (Ptrace code) and assure the required parameters for the accelerator operation. The small gap height used for the clamps provided reverse field distributions with fringe field of short extensions and no need for inactive clamps. The use of atypical geometry for the clamp coils solved the problem of lack of space. The fringe field distributions were measured with a Hall probe and are in good agreement with the predictions of the numerical calculations. The beam trajectories inside the magnets were determined using the floating wire technique and the results obtained agree within 0.1% with the calculated values. This technique is recommended when it is necessary to measure orbits in the absence of the beam.

### *Acknowledgments*

We would like to thank Dr. Maria Vittoria P. Heller for having kindly lent the pulley and for many informative discussions during this work. We also wish to express our thanks to Dr. Marcello Damy de Souza Santos for the important suggestions concerning the floating wire technique.

We would like to acknowledge the financial support from FAPESP, CNPq and FINEP.

### *References*

[1] Roy E. Rand, *Recirculating Electron Accelerators*, Harwood Academic Publishers, New York (1984).
[2] U. Vogel, *The Review of Scientific Instruments*, **36** (1965) 188.
[3] H. Babic and M. Sedlacek, *Nuclear Instruments and Methods*, **56** (1967) 170.
[4] H.A. Enge, *The Review of Scientific Instruments*, **35** (1964) 278.
[5] A. Septier, *Focusing of Charged Particles*, Academic Press Inc., New York (1967).
[6] M.T. Menzel and H.K. Stokes, Poisson Code, in: *Users Guide for the Poisson-Superfish Group of Codes*, Los Alamos National Laboratory, 1987.
[7] K.H. Kaiser, PTRACE, modified version of RAYTRACE (H. Enge and S. Kowalski), Mainz (1985).
[8] Herminghaus *et al.*, *Nuclear Instruments and Methods* **138** (1976) 12.
[9] L.R.P. Kassab, Projeto, construção e teste do sistema de ímãs principais do acelerador microtron booster do IFUSP, Ph.D. Thesis, IFUSP (1996).

[10] L.R.P. Kassab and P. Gouffon, The use of correcting coils in end magnets of accelerators, in: *Proceedings of Particle Accelerators Conference*, Vancouver, Canada, 1997.
[11] F.W. Bell, Hall Probe model DAP4-1835.
[12] F.W. Bell, Gaussmeter model 640.